PROCEEDINGS OF SCIENCE

Particle acceleration at reflected shocks in supernova remnants

Iurii Sushch,[a,b,*] **Jacobus F. Le Roux**[a] **and Robert Brose**[c]

[a] *Centre for Space Research, North-West University, 2520 Potchefstroom, South Africa*

[b] *Astronomical Observatory of Ivan Franko National University of Lviv, Kyryla i Methodia 8, 79005 Lviv, Ukraine*

[c] *Dublin Institute for Advanced Studies, Astronomy & Astrophysics Section, DIAS Dunsink Observatory, Dublin D15 XR2R, Ireland*

E-mail: iurii.sushch@nwu.ac.za

Supernovae remnants (SNRs) are widely considered to be the prime sources of Galactic cosmic rays (CRs). The efficient particle acceleration at the shocks of SNRs is indirectly confirmed by the detection of non-thermal emission across the whole electromagnetic spectrum from radio to very-high-energy gamma-rays. About 80% of all SNRs originate from core-collapse events and are expected to expand into a complex environment of the stellar wind bubble blown up by their progenitor stars, where the forward shock might interact with various density inhomogeneities. Such interactions would cause the formation of reflected shocks propagating back into the remnant which can potentially be strong enough to accelerate particles. Current investigations of particle acceleration in SNRs are usually limited to forward and reverse shocks ignoring the complexity of the hydrodynamic picture. Although for most SNRs the observed shell-like morphology generally agrees with an idea that high energy particles originate predominantly from the forward shock, precise spatially resolved measurements do not always agree with this simplified picture. This work is focused on the investigation of particle acceleration at the reflected shocks formed through the interaction of the forward shock with density inhomogeneities and its potential impact on the overall observational properties.

38th International Cosmic Ray Conference (ICRC2023)
26 July - 3 August, 2023
Nagoya, Japan

ICRC2023
38th International Cosmic Ray Conference
The Astroparticle Physics Conference

*Speaker

PoS(ICRC2023)262

1. Introduction

Most of supernova remnants (SNRs) are results of core-collapse explosion of massive stars which implies that they are expanding into stellar wind bubbles shaped by their progenitor stars. The circumstellar media (CSM) in which SNRs evolve are strongly inhomogeneous that can significantly impact the particle acceleration at the SNR shocks. Several recent works investigated in detail particle acceleration in SNRs expanding into different types of CSM depending on their progenitor stars [see e.g. 5, 7, 12], while in this study we would like to focus on the effects imposed reflected shocks that are formed during interactions of the forward shock of an SNR with termination shocks and/or contact discontinuities that are abundant in wind-shaped environments. Such reflected shocks propagate into the SNR interior and may further re-accelerate particles. Moreover, they can interact with the reverse shock and, bouncing off the contact discontinuity inside the SNR, with the forward shock impacting their dynamics and naturally affecting the particle acceleration. In the following we will discuss these effects and their potential observational signatures.

2. Simulation setup

This study is based on numeric simulations with the RATPaC (**R**adiation **A**cceleration and **T**ransport **Pa**rallel **C**ode) software which is designed to calculate the particle transport spatially (1-D, spherical symmetry), energy, and time-dependently using a kinetic approach [4, 11, 13–15]. In this section we briefly describe the code and the setup used in this particular study while for more details we refer to our previous works.

2.1 Hydrodynamics

The evolution of an SNR is described by solving standard gas-dynamical equations

$$\frac{\partial}{\partial t}\begin{pmatrix}\rho\\ \mathbf{m}\\ E\end{pmatrix}+\nabla\begin{pmatrix}\rho\mathbf{v}\\ \mathbf{m}\mathbf{v}+P\mathbf{I}\\ (E+P)\mathbf{v}\end{pmatrix}^{T}=\begin{pmatrix}0\\ 0\\ 0\end{pmatrix} \tag{1}$$

$$\frac{\rho\mathbf{v}^2}{2}+\frac{P}{\gamma-1}=E, \tag{2}$$

where ρ is the density of the thermal gas, $\mathbf{v}$ the plasma velocity,$\mathbf{m}=\mathbf{v}\rho$ the momentum density, P the thermal pressure of the gas and E the total energy density of the ideal gas with $\gamma=5/3$. We assume that the CR pressure and magnetic field are dynamically unimportant. The equations are solved in 1D for spherical symmetry in parallel to the particle transport equation using the PLUTO code [8].

2.2 Magnetic field

Upstream of the forward shock of the SNR the ambient magnetic field is assumed to be amplified by a factor $k=5$ and to exponentially decline on a length scale $\Delta l=0.05R_{\rm sh}$, until it reaches the field strength in the far-upstream medium.

Assuming a shock compression ratio of 4, the immediate downstream magnetic field is then given by

$$B_{\rm d} = \sqrt{11} k B_{\rm wind}(R_{\rm sh}) \tag{3}$$

The RATPaC code also allows for self-consistent calculation of magnetic turbulence upstream assuming resonant streaming instability [3] which was not used in this study.

2.3 Particle transport and acceleration

The time-dependent transport equation for the differential number density of cosmic rays N [10] is given by:

$$\begin{aligned}\frac{\partial N}{\partial t} =& \nabla(D_r \nabla N - \mathbf{u} N) \\ & - \frac{\partial}{\partial p}\left((N\dot{p}) - \frac{\nabla\cdot\mathbf{u}}{3} N p\right) + Q\,,\end{aligned} \tag{4}$$

where D_r denotes the spatial diffusion coefficient, $\mathbf{u}$ the advective velocity, $\dot{p}$ energy losses and Q the source of thermal particles. The equation is solved in 1D with spherical symmetry in a co-moving with the shock frame using the *FiPy*-library [6]. The outer grid boundary extends to 65 of shock radii upstream, so all accelerated particles can be kept in the simulation domain. The equation is solved in the test-particle approximation keeping the the CR pressure under 10% of the shock's ram pressure

To characterize particle injection We use the thermal leakage model [2],

$$Q = \chi n_{\rm u}(V_{\rm sh} - V_{\rm u})\delta(R - R_{\rm sh})\delta(p - p_{\rm inj}), \tag{5}$$

where χ is the injection efficiency parameter, $n_{\rm u}$ is the plasma number density in the upstream region, $V_{\rm sh}$ is the shock speed, $V_{\rm u}$ is the plasma speed upstream of the shock, $R_{\rm sh}$ is the shock radius, and $p_{\rm inj} = \xi p_{\rm th}$ is the injection momentum, defined as a multiple of the thermal momentum in the downstream plasma. The injection efficiency for the compression ratio of 4 is determined as

$$\chi = \frac{4}{\sqrt{\pi}} \frac{\xi^3}{e^{\xi^2}}. \tag{6}$$

The diffusion is assumed to scale with the Bohm diffusion coefficient

$$D(p) = \eta_{\rm B} \frac{pc^2}{3eB}, \tag{7}$$

where $\eta_{\rm B} \geq 1$ is the Bohm factor and a measure of acceleration efficiency. In this study we adopt the value $\eta_{\rm B} = 10$. In case of solving the transport equation for turbulence in parallel to the particle transport equation (see above) the diffusion coefficient can be calculated self-consistently. This utility of the RATPaC code was not used in this study.

2.4 Non-thermal radiation

Non-thermal radiation produced by accelerated particles is calculated using post-processing routines taking into account synchrotron, inverse Compton scattering, and hadronic interactions with subsequent pion decay. The latter relies on Monte Carlo event generators, namely DPMJET-III and UrQMD, for the calculation of inelastic cross-sections and differential production rates of secondary particles produced in nuclei collisions [1].

3. Results

We start our assessment of the impact of reflected shocks on particle acceleration and production on non-thermal emission from a closer look at the simulations presented in [12] for a generic SNR with a Wolf-Rayet (WR) progenitor. In this scenario, the SNR forward should would interact with the wind termination shock at relatively early stages triggering the formation of the reflected shock. In the next two subsections we discuss the effects caused by the reflected shock in this simulation. The last subsection exploits a different simulation setup focused on the acceleration at the reverse shock and the impact of the reflected shock once it reaches and boosts the reverse shock.

3.1 Compression and re-acceleration at the reflected shock

The forward shock reaches the WR wind termination shock at about 400 years resulting in the formation of the reflected shock which then propagates into the SNR interior. The 1 TeV electron density profiles shown in Fig. 3.1 illustrate a strong compression of particles at the reflected shock as it propagates inside the remnant. The pile-up of the electron density at around $0.94R_{\rm sh}$ for the 450-years profile (orange line) corresponds to the location of the reflected shock. The electron density at the reflected shock is roughly twice larger than the electron density at the forward shock. Observationally this would result in the gamma-ray and potentially radio/X-ray emission (depending on the distribution of the magnetic field) being associated with the reflected shock. In this case the size of the observed remnant could decrease with time. It would be however quite difficult to catch in observations due to the large timescales of this process.

We assessed a potential re-acceleration at the reflected shock by solving the transport equation with the adiabatic losses term $\left(\frac{\nabla\cdot\mathbf{u}}{3}Np\right)$, that governs particle acceleration, set to zero in the downstream (see Eq. 4). In this way we ignore any potential acceleration of particles at the reflected shock and the comparison to the full simulation would yield a net acceleration at the reflected shock. The resulting spectrum, however, appears to be identical to the one obtained in the full simulation implying that there is no addition re-acceleration of particles at the reflected shock. This is also not surprising given the high temperature of the shocked plasma in the downstream. Although the velocity of the reflected shock is very high its Mach number is low due to the high value of speed of sound in the hot medium.

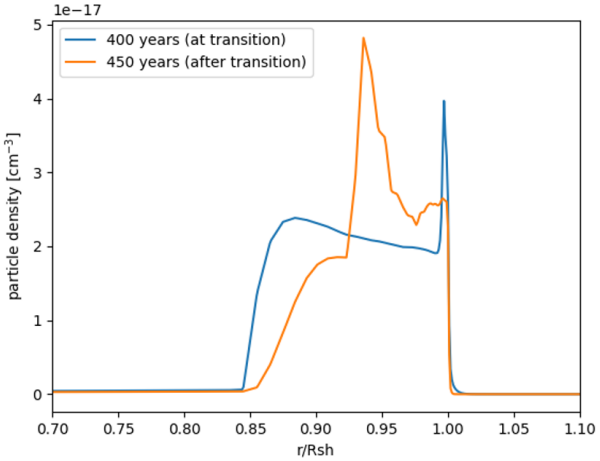

Figure 1: Radial profiles of 1 TeV electron density at two different times. The blue line (400 years) correspond to the moment of interaction of the forward shock with the wind termination shock, i.e. the moment of formation of the reflected shock. The orange line (450 years) shows the profile 50 years after the formation of the reflected shock and the evident pile-up of particles at around $0.94R_{\rm sh}$ corresponds to the location of the reflected shock.

3.2 Reflected-forward shock interactions

After the reflected shock bounces back from the contact discontinuity in the SNR interior it propagates outward towards the forward shock and moves faster than the forward shock. Eventually it catches up with the forward shock and accelerates it. This event yields an instantaneous increase of the maximum energy of accelerated electrons resulting in raise of the gamma-ray (especially above a TeV) and X-ray emission. The first such event happens at around 600 years but it repeats later on as the reflected shock keeps bouncing between the forward shock and the contact discontinuity. For the video that shows the evolution of the electron spectrum, radiation (synchrotron and inverse Compton) spectra, density and magnetic field profiles, and the shock velocity follow the link.

On Fig. 3.2 we present simulated light curves for the X-ray emission at 1 – 10 keV (red circles) and gamma-ray emission at high (HE; 1 – 100 GeV; blue circles), and very-high energies (VHE; above 1 TeV; orange circles). The sporadic spikes noticeable in the X-ray and VHE light curves correspond to the events of the reflected-forward shock interaction. During these events one can observe a very fast raise of the emission with the increase of the flux up to 100% in 10 years[1] followed by a slower decrease. Characteristic time scales for the simulated brightening suggest that these effects should be detectable even by current generation of instruments. In fact, it is possible that such an occurrence is observed in the Tycho SNR where the brighteting of the X-ray stripe was detected [9]. The detected brightening is accompanied by the hardening of the spectrum which could be interpreted by the increase of the maximum energy. Such a behaviour is well consistent with what one would expect in the event of the reflected-forward shocks interaction. It is however difficult to distinguish such an even from other possible mechanisms of X-ray brightening. A continuous monitoring of such events as well as simultaneous observations in the gamma-ray band would certainly help understanding their nature.

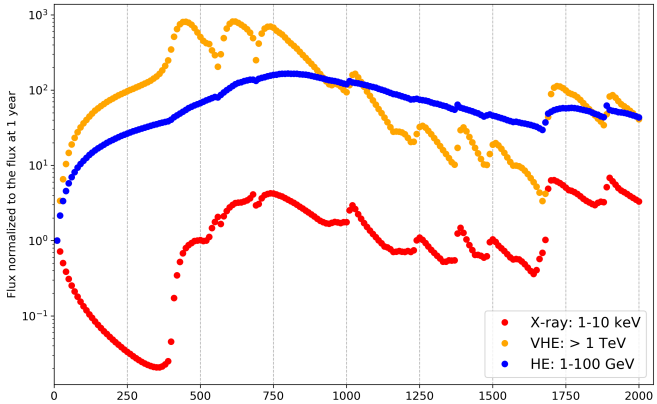

Figure 2: Simulated light curves for the time span of 2000 years for X-rays at 1 – 10 keV (red circles), the high-energy (HE) gamma-rays 1 – 100 GeV band (blue circles), and very-high-energy (VHE) gamma-rays above a TeV (orange circles). The gamma-ray emission is produced through the inverse Compton scattering of accelerated electrons. All light curves are normalized to the flux at 10 years. Every bin of the light curves correspond to a 10-year time step.

3.3 Boost of acceleration at the reverse shock

To study acceleration at the reverse shock and to assess the potential boost of acceleration due to the interaction of the reflected shock with the reverse shock we created a simplified setup where the SNR evolves in a constant density medium with a density jump by a factor of 10 at 1 pc. The

[1] 10 years is the span of one bin in the light curves

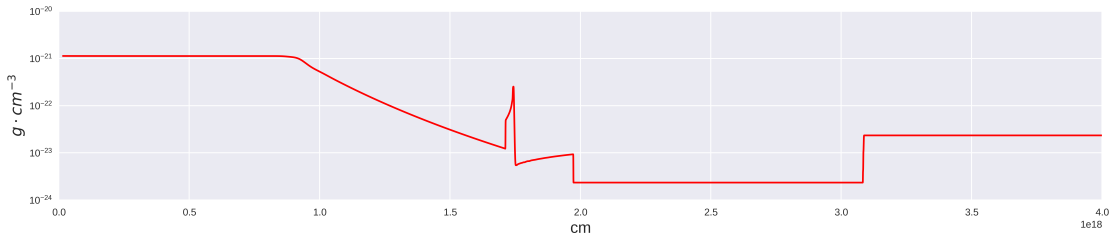

Figure 3: Density profile at 50 years for the test setup to study acceleration at the reverse shock. The ambient medium that the SNR is expanding to features a density jump by a factor of 10 at 1 pc from the centre.

Fig. 3 illustrates the density radial profile at 50 years of evolution when the forward shocks does not reach the density jump yet. As soon as the forward shock reaches the density jump at around 90 years (see the video under the link) the reflected shock is created and starts propagating into the interior. At around 110 years the reflected shock reaches the contact discontinuity and generates two more shocks: a transmitted shock that continues propagating towards the reverse shock and reflected shock that bounces back towards the forward shock. In the following we will focus only on the transmitted shock as we are interested in its interaction with the reverse shock. Hereafter, we refer to it as a reflected shock. At 120 years this shock reaches the reverse shock and accelerates the latter. Note, at this stage the shock that bounced back of the contact discontinuity towards the forward shock does not reach the forward shock yet.

We perform two simulation runs where in one run we inject particles at the forward shock and in the other we inject particles at the reverse shock. Figures 4 and 5 show the evolution of the proton spectrum accelerated at the forward and reverse shocks correspondingly. The spectra are shown for 70 (blue line), 120 (orange line), and 140 (green line) years. It can be seen that while for the forward shock the maximum energy is decreasing due to the deceleration of the sock for the reverse shock the maximum energy increases as the shock is hit by the reflected shock. At $\sim$ 120 years the maximum energy achievable at the forward and reverse shock is roughly the same. This test model suggests that at some point during the SNR evolution the acceleration at the reverse shock could be more efficient than at the forward shock due to the interaction with the reflected shock. This could be particularly the case for very late times when the SNR reaches the outer shell of the stellar wind bubble which results in significant weakening of the forward shock, while the reverse shock can still be strong and additionally boosted by reflected shocks [see also 5].

It should be noted, however, that the results obtained in this test model are parameter dependent. In particular the conclusions would strongly depend on the prescription of the magnetic field in the upstream of the reverse shock, i.e. in the the supernova ejecta. In the setup described above the magnetic field is assumed to be the same as in the upstream of the forward shock, which in reality could be different. In the future we plan to expand this work and carefully study the acceleration conditions at the reverse shock.

References

[1] Bhatt M., Sushch I., Pohl M., Fedynitch A., Das S., Brose R., Plotko P., Meyer D. M. A., 2020,

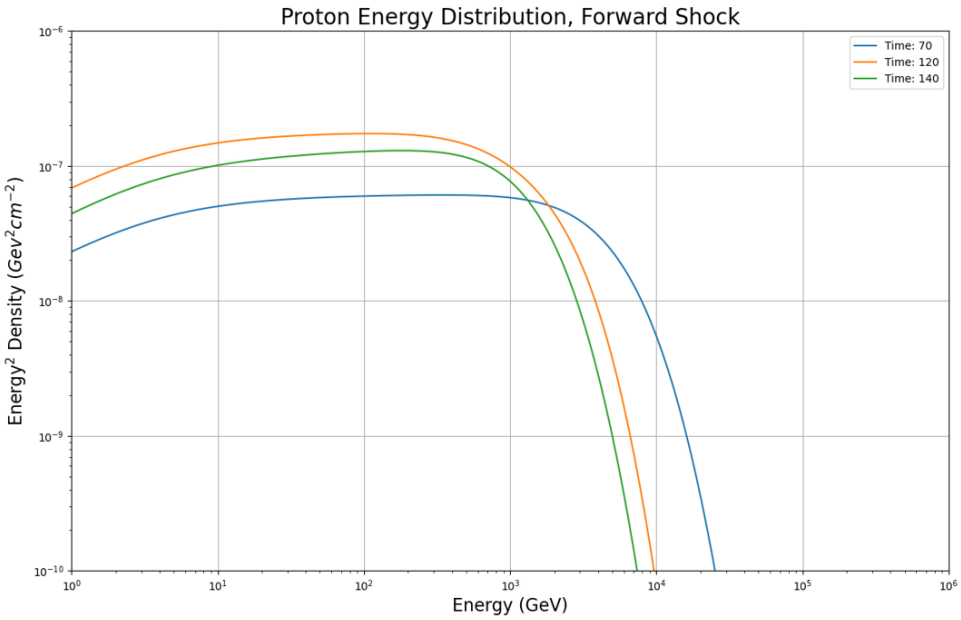

Figure 4: The volume averaged spectrum of protons injected and accelerated at the forward shock for 70 (blue line), 120 (orange line) and 140 (green line) years.

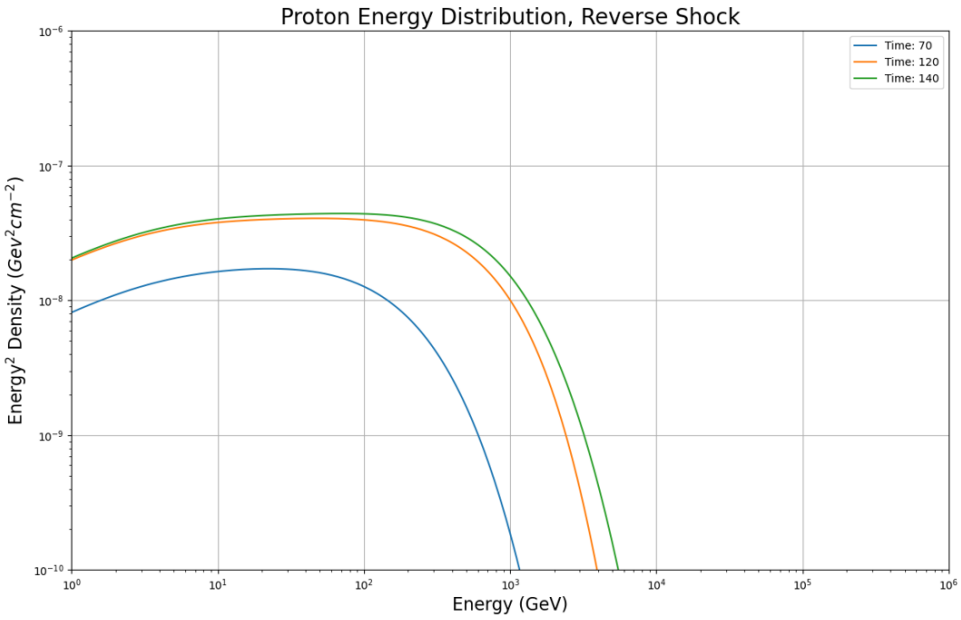

Figure 5: Same as Fig. 4 but for protons injected and accelerated at the reverse shock

Astroparticle Physics, 123, 102490

[2] Blasi P., Gabici S., Vannoni G., 2005, , 361, 907

[3] Brose R., Telezhinsky I., Pohl M., 2016, , 593, A20

[4] Brose R., Sushch I., Pohl M., Luken K. J., Filipović M. D., Lin R., 2019, , 627, A166

[5] Das S., Brose R., Meyer D. M. A., Pohl M., Sushch I., Plotko P., 2022, , 661, A128

[6] Guyer J. E., Wheeler D., Warren J. A., 2009, Computing in Science and Engineering, 11, 6

[7] Kobashi R., Yasuda H., Lee S.-H., 2022, ApJ, 936, 26

[8] Mignone A., Bodo G., Massaglia S., Matsakos T., Tesileanu O., Zanni C., Ferrari A., 2007, , 170, 228

[9] Okuno T., Tanaka T., Uchida H., Aharonian F. A., Uchiyama Y., Tsuru T. G., Matsuda M., 2020, , 894, 50

[10] Skilling J., 1975, , 172, 557

[11] Sushch I., Brose R., Pohl M., 2018, , 618, A155

[12] Sushch I., Brose R., Pohl M., Plotko P., Das S., 2022, , 926, 140

[13] Telezhinsky I., Dwarkadas V. V., Pohl M., 2012a, Astroparticle Physics, 35, 300

[14] Telezhinsky I., Dwarkadas V. V., Pohl M., 2012b, , 541, A153

[15] Telezhinsky I., Dwarkadas V. V., Pohl M., 2013, , 552, A102